IEEE Transactions on Automation Science and Engineering (T-ASE) paper, presented at ICRA 2024, Yokohama, Japan.
Cite as T-ASE paper.

Online Adaptive Motion Generation for Humanoid Locomotion on Non-Flat Terrain via Template Behavior Extension

Xiang Meng, Zhangguo Yu, Xuechao Chen, Zelin Huang, Fei Meng, and Qiang Huang, *Fellow, IEEE*

***Abstract*— For humanoid robots, online motion generation on non-flat terrain remains an ongoing research challenge. Computational complexity is one of the primary restrictions that preclude motion planners from generating adaptive behaviors online. In this paper, we investigate this problem and decompose it into two sequential components: an Efficient Behavior Generator (EBG) and a Nonlinear Centroidal Model Predictive Controller (NC-MPC). The EBG is responsible for optimizing the physically feasible whole-body template behaviors, which can provide reliable warm-starts for NC-MPC, thereby greatly reducing the computational effort of online planning. With tailored objective function and feet complementary constraints, the EBG can search for a near-optimal solution after several iterations within seconds for different behaviors including walking, running, and jumping, even with intuitive initial guesses. To make the template behaviors extensible when the robot encounters possible different scenarios, the NC-MPC is proposed to regenerate the reactive motion online to adapt it to the real local environment. Finally, we validate the effectiveness of synthesizing EBG and NC-MPC for humanoid locomotion on non-flat terrain in simulation and on the real humanoid robot BHR7P.**

***Note to Practitioners*— For current humanoid robots, dynamically traversing non-flat terrain such as stairs, slopes, and gaps in the real world presents a significant challenge. In this paper, we propose an adaptive motion planner for humanoid robots to traverse non-flat terrain, which is properly integrated into the closed loop of online control. Considering computational complexity and motion extensibility, the planner consists of two parts: an efficient behavior generator performed offline and a nonlinear model predictive controller performed online. The behavior generator can efficiently generate template behaviors for the humanoid robot, including various gaits such as walking, running, and jumping. To make these template behaviors adaptable, a nonlinear model predictive controller based on the centroidal dynamics model is developed to plan reactive motions online. It can extend template behaviors to fit potentially different scenarios in practice. The proposed method is validated in simulations and experiments with the humanoid robot BHR7P. Furthermore, this method can be applied to legged robots or systems that need to move dynamically on non-flat terrain, such as quadruped and hexapod robots.**

***Index Terms*— Humanoid locomotion, motion generation, trajectory optimization, model predictive control.**

Manuscript received 12 September 2023; accepted 17 October 2023. This article was recommended for publication by Associate Editor J. Gu and Editor P. Rocco upon evaluation of the reviewers' comments. This work was supported in part by the National Natural Science Foundation of China under Grant 62073041 and Grant 61973039 and in part by the 111 Project under Grant B08043. *(Corresponding author: Zhangguo Yu.)*

Xiang Meng and Zelin Huang are with the School of Mechatronical Engineering, Beijing Institute of Technology (BIT), Beijing 100081, China.

Zhangguo Yu, Xuechao Chen, Fei Meng, and Qiang Huang are with the School of Mechatronical Engineering, Beijing Institute of Technology, Beijing 100081, China, also with the Key Laboratory of Biomimetic Robots and Systems, Ministry of Education, Beijing 100081, China, and also with the National Key Lab of Autonomous Intelligent Unmanned Systems, Beijing 100081, China (e-mail: yuzg@bit.edu.cn).

This article has supplementary material provided by the authors and color versions of one or more figures available at https://doi.org/10.1109/TASE.2023.3327819.

Digital Object Identifier 10.1109/TASE.2023.3327819

I. Introduction

HUMANOID robots are widely recognized as the most promising candidates to replace humans in complex or hazardous work environments. Over the decades, humanoid robots have developed the ability to move stably on flat ground [1], [2], [3], [4], [5]. However, planning physically feasible dynamic locomotion online on non-flat terrain remains a significant challenge [6], [7], [8], [9], [10]. To achieve the desired locomotion on non-flat terrain, it is tedious and time-consuming (relative to the robot's control period) to simultaneously compute feasible whole-body behaviors and contact forces in real-time while adhering to some restrictive constraints, such as the unilateral contact forces and the Range of Motion (RoM) of the robot joints.

There are some successful pattern generators using simplified models such as the Linear Inverted Pendulum Model (LIPM) and its extended variants [1], [3], [4]. The robot is usually represented as an inverted pendulum, and the contact force is substituted by the Zero Moment Point (ZMP) [11] to control the Center of Mass (CoM). Due to the simplified dynamic equations, these generators can rapidly compute the CoM trajectory when provided desired ZMP trajectories, rendering them suitable for online Model Predictive Control (MPC) [12], [13]. However, taking ZMP as a stability criterion of the humanoid robot is subject to two restrictive assumptions: first, that both feet are on flat or coplanar planes, and second, that the friction coefficient of contacts is infinite, i.e., the feet do not slide. These assumptions make it challenging to adapt these efficient planners to non-flat terrain.

To plan the desired behavior on non-flat terrain, some methods have incorporated the full rigid body dynamics model into motion planning. Despite the high computational complexity, the behaviors optimized by these methods are dynamic and graceful [14], [15], [16]. Unfortunately, such approaches typically require solving high-dimensional nonconvex optimization problems, which can take several minutes, or even

IEEE Transactions on Automation Science and Engineering (T-ASE) paper, presented at ICRA 2024, Yokohama, Japan.

hours, to obtain feasible solutions. This fundamentally restricts their application for online adaptive motion generation.

In recent years, some studies [17], [18] have demonstrated that under the mild assumption that the actuated joints of the robot can provide sufficient torque, the centroidal dynamics model [19] can be used to plan physically feasible movements and contact forces. Using trajectory optimization (TO) [20], the centroidal dynamics model and its variants have been exploited to generate impressive behaviors for biped and quadruped robots [21], [22], [23], [24], [25], [26], [27], [28], [29], including validations on real hardware.

Using the centroidal dynamics model, these motion generators commonly split whole-body motion planning into two iterative optimization problems: centroidal momentum optimization and whole-body kinematics optimization, such as kino-dynamic planning [27]. Carpentier et al. [22] used dedicated multi-shooting method to tackle the bilinear terms of the centroidal momentum dynamics to optimize the momentum trajectory efficiently. Dai and Tedrake [26] resolved the nonconvex momentum dynamics by minimizing an approximated convex upper bound on the l_1 centroidal angular momentum norm with convex optimization. Ponton et al. [27] proposed an efficient algorithm for behavior generation with sequential convex approximations of the centroidal dynamics, which reveals the potential for efficient planning with receding horizon control. Meduri et al. [28] proposed a nonlinear model predictive control framework for motion planning by exploiting the biconvex structure of the centroidal dynamics. Compared to methods using the full rigid body dynamics model, these approaches require less computational effort due to fewer decision variables and constraints in the suboptimizations. However, these approaches often rely on first planning a relatively long-horizon motion offline and then naively tracking it online, rather than properly incorporating the motion planners into the closed loop of online control.

There are also some interesting attempts to plan online adaptive motion by building an offline gait library [30], [31]. According to the online walking speed commands, these methods select the appropriate gait online, or update it, from a library of periodic gaits including different step lengths and periods. It significantly reduces the complexity of online trajectory optimization. While these methods allow the bipedal robots to plan reactive motion online on non-flat terrain, the elements in the gait library are dense and not sufficiently extensible.

In this article, to tackle the above mentioned problems, an online adaptive motion planner for humanoid robots on non-flat terrain is proposed. Considering the computational expediency, we split the online motion generation into two sequential optimization problems, which are an Efficient Behavior Generator (EBG) and a Nonlinear Centroidal MPC (NC-MPC), as illustrated in Fig. 1. The EBG is performed offline and optimizes physically feasible whole-body template behaviors by solving a large-scale nonlinear TO problem. Instead of simply tracking the template behaviors, the NC-MPC is proposed to improve the extensibility of optimized behaviors when the robot encounters possible different scenarios. Given desired footholds from the high-level contact planner (e.g. [32]), the NC-MPC takes the appropriate template behavior as a warm-start and recomputes adaptive centroidal motion and contact forces online to adapt to the local environment.

The decomposition between EBG and NC-MPC is a good compromise in terms of computational expediency and behavior extensibility. On the one hand, the EBG greatly reduces the online computational effort and the template behaviors enable the NC-MPC to run fast and feasible. On the other hand, the NC-MPC provides a proper way to extend the template behaviors and to regenerate adaptive motion online for often different scenarios.

The main contributions of this article are as follows:

1) We design a generic and efficient whole-body dynamic template behavior generator with a unified objective function and tailored feet complementary constraints. Our generator can search for a near-optimal solution after several iterations within seconds, even with intuitive initial guesses, when planning different behaviors including walking, running, and jumping.
2) A nonlinear centroidal MPC is proposed to plan online adaptive centroidal motion and contact forces on non-flat terrain via template behavior extension. It can extend the optimized template behaviors to directly adapt to possible different scenarios online rather than re-optimizing behaviors before execution.

The rest of this article is organized as follows. Section II describes the trajectory optimization formulation of the EBG in detail. Section III presents the construction of the NC-MPC. Section IV presents some simulation and experiment results with the humanoid robot BHR7P, including walking, running, and jumping behaviors on non-flat terrain. Section V discusses the limitations of the current approach and potential solutions for future work. Finally, Section VI concludes this article.

II. Efficient Behavior Generator

A. Overview

We transcribe the whole-body template behavior generation as a nonlinear TO problem. The goal of TO is that when the terrain information and the nominal footholds are provided, it can automatically determine the CoM, centroidal linear and angular momentum, contact forces, optimal footholds, step timings, and whole-body motion consistent with the centroidal solution. In addition, it is expected to have a versatile objective function for generating different behaviors rather than every new behavior requiring a specific hand-crafted objective function. In other words, only the constraints need to be changed when planning different behaviors.

B. Centroidal Dynamics and Whole-Body Kinematics Model

According to the Newton-Euler equations, centroidal dynamics can be represented as follows

$$\dot{\boldsymbol{x}} = \begin{bmatrix} \dot{\boldsymbol{c}} \\ \dot{\boldsymbol{l}} \\ \dot{\boldsymbol{h}} \end{bmatrix} = \begin{bmatrix} \boldsymbol{l}/m \\ \sum_i \sum_j \boldsymbol{f}_i^j + m\boldsymbol{g} \\ \sum_i \sum_j (\boldsymbol{p}_i + \boldsymbol{R}_i(\boldsymbol{\phi}_i + \boldsymbol{\varphi}_i^j) - \boldsymbol{c}) \times \boldsymbol{f}_i^j \end{bmatrix} \quad (1)$$

IEEE Transactions on Automation Science and Engineering (T-ASE) paper, presented at ICRA 2024, Yokohama, Japan.

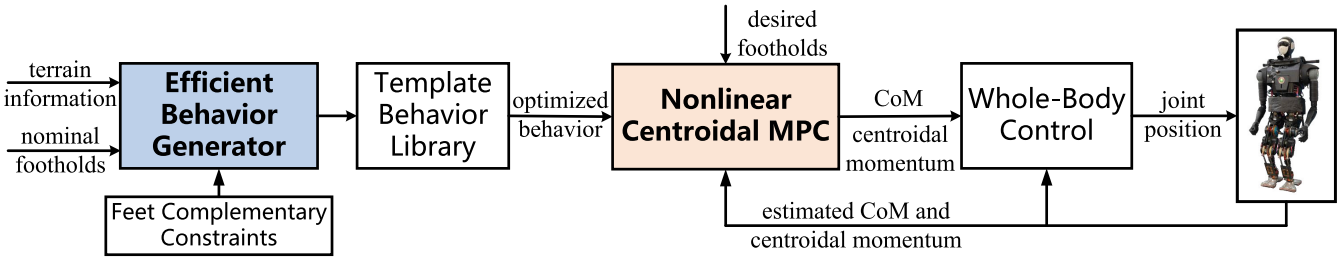

Fig. 1. Algorithm framework. First, given the terrain information and nominal footholds, the physically feasible whole-body motion can be optimized by the Efficient Behavior Generator with tailored feet complementary constraints and then listed in the template behavior library. Second, warmed up by the optimized behavior instead of naively tracking it, a Nonlinear Centroidal MPC is developed to extend the template behavior and regenerate adaptive motions according to the desired footholds from the high-level contact planner and estimated centroidal states. Finally, the whole-body control tracks the centroidal solutions from the NC-MPC and computes the desired joint position for the humanoid robot. This article focuses on motion generation, including the EBG (blue box) and the NC-MPC (red box).

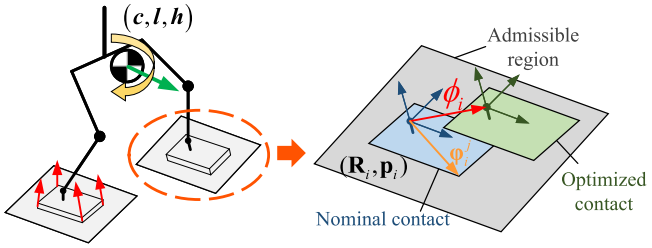

Fig. 2. Centroidal dynamics model and footholds optimization.

where $\boldsymbol{c} \in \mathbb{R}^3$ is the position of CoM, $\boldsymbol{l} \in \mathbb{R}^3$ and $\boldsymbol{h} \in \mathbb{R}^3$ are centroidal linear and angular momentum, respectively, m is the total mass of the robot, $\boldsymbol{g} = [0, 0, -9.81]^T$ is the gravity vector, $(\boldsymbol{R}_i, \boldsymbol{p}_i) \in SE(3)$ is the desired orientation and nominal ankle position of i-th contact foot, $\boldsymbol{\phi}_i \in \mathbb{R}^3$ is the admissible foot contact region on contact surfaces, $\boldsymbol{\varphi}_i^j \in \mathbb{R}^3$ is the j-th contact point's location of i-th foot, note that $\boldsymbol{\phi}_i$ and $\boldsymbol{\varphi}_i^j$ are both expressed in the local frame of the i-th foot, as illustrated in Fig. 2.

In (1), it presents the relationship between the rate of centroidal state and contact forces at each contact point. If we directly optimize the centroidal states and contact forces in TO, it will be troublesome in the following: 1) It is difficult to intuitively evaluate the optimized centroidal solution. 2) When the centroidal solution is mapped to the joint space, there is a risk that the position and velocity of the joints potentially exceed the RoM in order for motion consensus.

Some recent works use kino-dynamics optimization to resolve these restrictions [25], [27]. However, they usually require heuristics to select proper parameters for iterative optimization between the centroidal momentum and the whole-body kinematics. In this article, we integrate the whole-body kinematics model into the centroidal momentum optimization like [21]. Consequently, we explicitly impose the constraints indicated below to enforce the whole-body motion to be consistent with the centroidal motion

$$\boldsymbol{c} = f_{CoM}(\boldsymbol{q}) \tag{2a}$$

$$\begin{bmatrix} \boldsymbol{l} \\ \boldsymbol{h} \end{bmatrix} = \boldsymbol{A}_G(\boldsymbol{q})\dot{\boldsymbol{q}} \tag{2b}$$

where $\boldsymbol{q}, \dot{\boldsymbol{q}} \in \mathbb{R}^{6+n}$ are the generalized position and velocity of the robot, f_{CoM} denotes the function that computes the position of CoM according to the robot configuration, $\boldsymbol{A}_G(\boldsymbol{q}) \in \mathbb{R}^{6\times(6+n)}$ is the centroidal momentum matrix [19].

Note that, as the whole-body kinematics model is considered, it is possible to directly constrain the position and posture of any link of the robot in TO, which is essential for the design of feet complementary constraints described in Section II-C.

C. Tailored Feet Complementary Constraints

The feet are the main parts of the robot's interaction with the external environment. A key observation is that the representation of the contact forces and the appropriate constraints on the swing foot have a significant effect on the convergence of the TO. We call this the feet complementary constraints and it is similar to the Linear Complementary Problem (LCP) [33], which compels that either the contact force is zero or the velocity of the contact point is zero and can be written as

$$\boldsymbol{f}_i^j \dot{\boldsymbol{p}}_i^j = \boldsymbol{0} \tag{3}$$

where $\dot{\boldsymbol{p}}_i^j$ denotes the velocity of the j-th contact point of the i-th foot.

Different from the LCP, in this paper, we focus on the representation of contact forces and the constraints on swing foot to enhance the performance of TO.

There are some common approaches to represent the contact forces, such as ZMP, Center of Pressure (CoP), and Contact Wrench Cone (CWC) [34], [35]. As illustrated in Fig. 2, the contact forces are exerted on the four corners of the rectangular foot. Instead of constraining the forces to stay in the CWC to ensure static equilibrium, for simplicity, the force at each contact point is restrained in the friction cone to prevent the foot from sliding on the contact surface. In practice, the friction cone is often approximated by an inner linearized friction pyramid to simplify the problem, just as shown on the left of Fig. 3. The linearized friction cone constraint is given by

$$\boldsymbol{\Psi}\boldsymbol{f} \leq \boldsymbol{0} \Leftrightarrow \begin{bmatrix} -1 & 0 & -\mu \\ 1 & 0 & -\mu \\ 0 & -1 & -\mu \\ 0 & 1 & -\mu \end{bmatrix} \begin{bmatrix} f^{t_1} \\ f^{t_2} \\ f^n \end{bmatrix} \leq \boldsymbol{0} \tag{4}$$

where f^{t_1}, f^{t_2} and f^n are the forces in the tangential and normal direction of the contact surface, respectively. Note that $\mu = \mu_{real}/\sqrt{2}$, and μ_{real} is the real friction coefficient.

IEEE Transactions on Automation Science and Engineering (T-ASE) paper, presented at ICRA 2024, Yokohama, Japan.

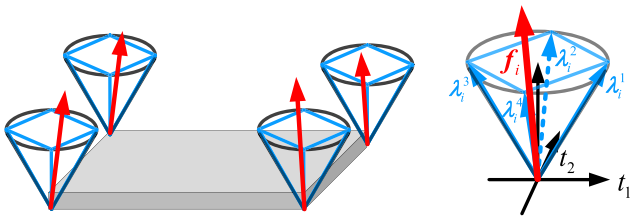

Fig. 3. Left: The linearized friction cones at four vertices of the rectangular foot. Right: The force is represented by the span form of the linearized friction pyramid.

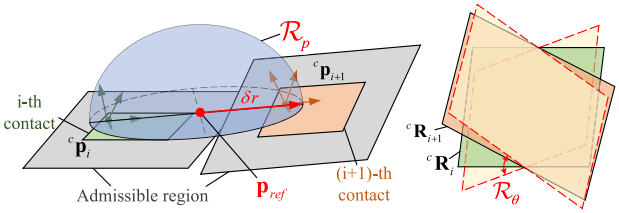

(a) Motion range (b) Posture range

Fig. 4. Constraints on the swing foot.

Instead of typically imposing the constraint (4) explicitly in many works [21], [22], [23], we resort to the span form of the linearized friction pyramid using the *double description method* [36] to represent this constraint implicitly in our TO. Note that the matrix $\mathbf{\Psi}$ is the face form of the linearized friction polyhedral. Using the *cdd* library [36], the transformation from the face form to the span form is given by

$$\mathbf{\Xi} = span(\mathbf{\Psi}) = \begin{bmatrix} \mu & \mu & -\mu & -\mu \\ \mu & -\mu & \mu & -\mu \\ 1 & 1 & 1 & 1 \end{bmatrix} \tag{5}$$

where the matrix $\mathbf{\Xi}$ is the span form of the linearized friction polyhedral, the $span()$ is the function in *cdd* library that calculates the span form of the polyhedral given its face form. Then the force can be indicated as a non-negative combination of the spans of the polyhedral cone

$$\boldsymbol{f}_i^j = \mathbf{\Xi}\boldsymbol{\alpha}_i^j = \sum_{s=1}^{4} \alpha_{i,j}^s \boldsymbol{\lambda}_{i,j}^s, \alpha_{i,j}^s \geq 0 \tag{6}$$

where the $\boldsymbol{\alpha}_i^j$ is a bunch of non-negative factors $\alpha_{i,j}^s$, the $\boldsymbol{\lambda}_{i,j}^s$ is the s-th column of the matrix $\mathbf{\Xi}$. Equation (6) governs the force that never violates the friction constraint, as illustrated on the right of Fig. 3.

We take the non-negative factors $\alpha_{i,j}^s$ as the decision variables in the optimization. Although the number of decision variables increases by one compared with directly using the force $\boldsymbol{f}_i^j$, the number of inequality constraints decreases from four to zero (only the upper and lower bounds of $\alpha_{i,j}^s$ need to be constrained). Importantly, it can promote the solving speed of the TO with fewer active set changes. Note that the scope of inequality constraints primarily pertains to the inequality relationship between decision variables, excluding considerations for the upper and lower bound constraints of decision variables.

To achieve different behaviors, the constraints on the swing foot also play an important role in our TO. For the sake of simplicity and generality, the constraints are presented with an example of walking on non-flat terrain. Since the whole-body kinematics model is incorporated into the optimization, it is straightforward to compute the position and posture $(\boldsymbol{R}_i, \boldsymbol{p}_i)$ of the swing foot with forward kinematics. Given the detailed terrain information such as $p^z = f_{terrain}(p^x, p^y)$, we impose clearance constraints on the points at the four corners of the swing foot to avoid collisions with the external environment

$$p_{i,j}^z - f_{terrain}(p_{i,j}^x, p_{i,j}^y) \geq \delta \tag{7}$$

where $\boldsymbol{p}_{i,j} = (p_{i,j}^x, p_{i,j}^y, p_{i,j}^z)$ is the coordinate of j-th corner of the swing foot, δ is the minimum clearance, in the TO, $\delta = 0.01m$.

As for the kinematics reachability, we restrict the swing foot moving within a hemispherical space shown in Fig. 4(a). The volume of the hemisphere relies on the deviation of the adjacent nominal footholds. The constraints are as follows

$$\begin{aligned} \boldsymbol{p}_i \in \mathcal{R}_p \;&\Leftrightarrow\; \left|\boldsymbol{p}_i - \boldsymbol{p}_{ref}\right| \leq \delta r \\ \boldsymbol{p}_{ref} &= \frac{1}{2}({}^c\boldsymbol{p}_i + {}^c\boldsymbol{p}_{i+1}) \\ \delta r &= \left|\frac{1}{2}({}^c\boldsymbol{p}_{i+1} - {}^c\boldsymbol{p}_i)\right| + \zeta \end{aligned} \tag{8}$$

where $\boldsymbol{p}_i$ is the ankle position of the swing foot, $\mathcal{R}_p$ denotes the range of motion, i.e., the hemisphere, $\boldsymbol{p}_{ref}$ is the center of the hemisphere, δr is the radius of the hemisphere, ${}^c\boldsymbol{p}_i$ and ${}^c\boldsymbol{p}_{i+1}$ are the positions of the adjacent nominal footholds, $\zeta \in (0.05\ m, 0.25\ m)$ is the slack margin that can be manually adjustable.

When the robot is moving on non-flat terrain, the posture of the swing foot should be aligned with the desired posture at the end of the swing phase. The posture constraints are similar to the motion constraints. A blend value is introduced to compute a time-varying desired posture with the predefined adjacent contacts. Then the attitude of the swing foot is enforced to stay close to the desired posture, as presented in Fig. 4(b). The posture constraints are given by

$$\begin{aligned} \boldsymbol{R}_i \in \mathcal{R}_\theta \;&\Leftrightarrow\; \boldsymbol{\xi}_i^T \boldsymbol{\xi}_d \in [\cos\theta, 1] \\ \boldsymbol{\xi}_i = \mathcal{T}_{\boldsymbol{R}}^{\boldsymbol{\xi}}(\boldsymbol{R}_i),\ \boldsymbol{\xi}_d &= \mathcal{T}_{\boldsymbol{R}}^{\boldsymbol{\xi}}(\gamma\, {}^c\boldsymbol{R}_i + (1-\gamma)\, {}^c\boldsymbol{R}_{i+1}) \end{aligned} \tag{9}$$

where $\boldsymbol{R}_i$ is the rotation matrix of the swing foot, $\mathcal{R}_\theta$ denotes the posture range, $\boldsymbol{\xi}_i \in \mathbb{R}^4$ is the quaternion of the swing foot, $\mathcal{T}_{\boldsymbol{R}}^{\boldsymbol{\xi}}$ is the transformation from rotation matrix to a quaternion, $\boldsymbol{\xi}_d$ is the quaternion of the desired posture which is a blend posture related to the adjacent contacts ${}^c\boldsymbol{R}_i$ and ${}^c\boldsymbol{R}_{i+1}$, $\gamma \in (0, 1)$ is a blend value that decreases linearly from 1 to 0 during swinging, $\theta \in (0, 0.15\ rad)$ is the admissible tolerance of the quaternion between the actual and the desired posture.

D. Direct Multi-Phase Trajectory Optimization

Once the above preparations are complete, the multi-phase movement from the initial state to the desired state can be written as the following Optimal Control Problem (OCP):

$$\min_{\substack{\boldsymbol{x},\boldsymbol{\phi},\boldsymbol{\alpha},\\ \boldsymbol{q},\dot{\boldsymbol{q}}}} \int_0^T (\|\boldsymbol{h}\|_{\boldsymbol{Q}_h}^2 + \|\ddot{\boldsymbol{c}}\|_{\boldsymbol{Q}_{\ddot{c}}}^2 + \sum_i \sum_j \left\|\boldsymbol{f}_i^j\right\|_{\boldsymbol{Q}_f}^2 + \|\tilde{\boldsymbol{q}}\|_{\boldsymbol{Q}_q}^2) dt \tag{10a}$$

IEEE Transactions on Automation Science and Engineering (T-ASE) paper, presented at ICRA 2024, Yokohama, Japan.

$$\text{s.t. } \dot{\boldsymbol{x}} = f(t, \boldsymbol{x}, \boldsymbol{f}_i^j), \quad \forall t \tag{10b}$$
$$\boldsymbol{\phi}_i \in \mathcal{S}_i, \quad t \in \mathcal{C}_i \tag{10c}$$
$$\boldsymbol{c} = f_{CoM}(\boldsymbol{q}), \quad \forall t \tag{10d}$$
$$\begin{bmatrix} \boldsymbol{l} \\ \boldsymbol{h} \end{bmatrix} = \boldsymbol{A}_G(\boldsymbol{q})\dot{\boldsymbol{q}}, \quad \forall t \tag{10e}$$
$$\boldsymbol{R}_i = \boldsymbol{R}_i^{\text{nom}}, \ \boldsymbol{p}_i = \boldsymbol{p}_i^{\text{nom}}, \ \alpha_{i,j}^s \geq 0, \ t \in \mathcal{C}_i \tag{10f}$$
$$\boldsymbol{R}_i \in \mathcal{R}_\theta, \ \boldsymbol{p}_i \in \mathcal{R}_p, \ \alpha_{i,j}^s = 0, \ t \notin \mathcal{C}_i \tag{10g}$$
$$\begin{bmatrix} \underline{\boldsymbol{q}} \\ \underline{\dot{\boldsymbol{q}}} \end{bmatrix} \leq \begin{bmatrix} \boldsymbol{q} \\ \dot{\boldsymbol{q}} \end{bmatrix} \leq \begin{bmatrix} \overline{\boldsymbol{q}} \\ \overline{\dot{\boldsymbol{q}}} \end{bmatrix}, \quad \forall t \tag{10h}$$
$$\boldsymbol{q}(0) = \boldsymbol{q}_{init}, \ \dot{\boldsymbol{q}}(0) = \boldsymbol{0}_{6+n} \tag{10i}$$
$$\boldsymbol{q}(T) = \boldsymbol{q}_{des}, \ \dot{\boldsymbol{q}}(T) = \boldsymbol{0}_{6+n} \tag{10j}$$
$$\ddot{\boldsymbol{c}}(0) = \ddot{\boldsymbol{c}}(T) = \dot{\boldsymbol{h}}(0) = \dot{\boldsymbol{h}}(T) = \boldsymbol{0}_3 \tag{10k}$$

where the decision variables include the CoM, the centroidal linear and angular momentum, footholds, non-negative factors of the contact forces, and the generalized position and velocity of the robot, T denotes the sum of the duration of all phases. The objective function includes the penalty of centroidal angular momentum, the acceleration of the CoM, the contact forces, and the deviation of the generalized position from the reference state. $\boldsymbol{Q}_h \in \mathbb{R}^{3\times3}$, $\boldsymbol{Q}_{\ddot{c}} \in \mathbb{R}^{3\times3}$, $\boldsymbol{Q}_f \in \mathbb{R}^{3\times3}$, $\boldsymbol{Q}_q \in \mathbb{R}^{(6+n)\times(6+n)}$ are the semi-positive definite matrix. $\tilde{\boldsymbol{q}} \triangleq \boldsymbol{q} - \boldsymbol{q}_{ref}$ is the deviation of the generalized position and $\boldsymbol{q}_{ref}$ is the reference of the state which can be a simple linear interpolation from the initial state $\boldsymbol{q}_{init}$ to the desired state $\boldsymbol{q}_{des}$. The constraints contain the centroidal dynamics (10b) corresponding to (1), the admissible contact region of the feet $\mathcal{S}_i$ during contact phases $\mathcal{C}_i$ (10c), the consistency between centroidal motion and whole-body motion (10d-10e), tailored feet complementary constraints for contact phases and swing phases (10f-10g), the bounds on the generalized position and velocity (10h) of the robot, and the boundary constraints on the robot state and the rate of centroidal momentum (10i-10k).

Note that although the initial and desired states of the robot are constrained to be stationary, this does not affect the generality of the OCP. It can also be implemented to optimize periodic gaits by applying periodic constraints.

We use the direct collocation method to transcribe the infinite-dimensional continuous-time OCP (10) into a Nonlinear Programming (NLP) problem with a finite number of decision variables and constraints. The OCP is discretized into N knots and the time intervals between two adjacent knots $\Delta t(i)$ are integrated into the decision variables of the NLP to optimize the step timings.

Considering the sparsity of the analytic gradients, we use the trapezoid method [20] to approximate the dynamics constraints and the generalized velocity:

$$\boldsymbol{x}[i+1] = \boldsymbol{x}[i] + \frac{\Delta t[i]}{2}(\dot{\boldsymbol{x}}[i+1] + \dot{\boldsymbol{x}}[i]) \tag{11}$$
$$\boldsymbol{q}[i+1] = \boldsymbol{q}[i] + \frac{\Delta t[i]}{2}(\dot{\boldsymbol{q}}[i+1] + \dot{\boldsymbol{q}}[i]) \tag{12}$$

III. Nonlinear Centroidal MPC to Extend Template Behaviors

The EBG can optimize a physically feasible whole-body trajectory offline with provided terrain information and nominal footholds. In practice, however, the robot often encounters different scenarios. An intuitive approach is to use the EBG to regenerate a new trajectory for adaptability. If we take the example of climbing a slope, in this way, we have to prepare a trajectory for every possible tilted angle and footholds before online execution, which means the motion planner becomes less useful at some point. In other words, it is hoped that the optimized template behaviors are of good extensibility. To this end, we propose a nonlinear centroidal MPC warmed up by the proper template behavior to regenerate adaptive motions online when the robot encounters possible different scenarios.

A. Centroidal Prediction Model

Considering online computational efficiency, we choose the centroidal dynamics model as the prediction model. Since the high-level contact planner can provide the desired footholds, under the mild assumptions that the contact sequence and step timings are given, it is easy to define an integer variable $\Lambda_i^j(t) \in \{0, 1\}$ for each contact point to indicate whether it is in contact or not. For example, $\Lambda_i^j(t) = 1$ indicates that the j-th contact of the i-th foot is active at the time t, while $\Lambda_i^j(t) = 0$ the contact is not active. The centroidal dynamics model can be rewritten as

$$\dot{\boldsymbol{x}} = \begin{bmatrix} \dot{\boldsymbol{c}} \\ \dot{\boldsymbol{l}} \\ \dot{\boldsymbol{h}} \end{bmatrix} = \begin{bmatrix} \boldsymbol{l}/m \\ \sum_i \sum_j \Lambda_i^j \boldsymbol{f}_i^j + m\boldsymbol{g} \\ \sum_i \sum_j (\boldsymbol{p}_i + \boldsymbol{R}_i\boldsymbol{\varphi}_i^j - \boldsymbol{c}) \times \Lambda_i^j \boldsymbol{f}_i^j \end{bmatrix} \tag{13}$$

Note that the contact force and the linearized friction constraints are still represented implicitly by (6). Different from the Equation (1), the local allowable translation variable $\boldsymbol{\phi}_i$ is removed to keep a consistent number of variables in the prediction horizon.

Thus, the decision variables of NC-MPC are the CoM $\boldsymbol{c}$, the centroidal linear and angular momentum $\boldsymbol{l}, \boldsymbol{h}$, and the non-negative factors $\alpha_{i,j}^s$ of the contact forces.

B. Objective Function and Constraints

The objective function takes advantage of the optimized template behaviors from EBG, including the penalty of deviation of the centroidal state and the regularization of contact forces.

1) Penalty of the Deviation of Centroidal State: The NC-MPC is expected to regenerate the feasible solution online that is close to the template behavior. Thus, it is intuitive to minimize the norm of the error between the predicted CoM position and the reference trajectory:

$$\Gamma_{CoM} = \left\| \boldsymbol{c} - \boldsymbol{c}^{ref} \right\|_{\boldsymbol{W}_{CoM}}^2 \tag{14}$$

where $\boldsymbol{c}^{ref}$ is the reference CoM trajectory, $\boldsymbol{W}_{CoM}$ is a positive definite diagonal weighted matrix.

We also penalize the error of the centroidal momentum, and it is observed that the inclusion of this penalty term can promote the rapid convergence of the NC-MPC. The penalty for the error of the Centroidal Momentum (CM) is given by

$$\Gamma_{CM} = \left\| \boldsymbol{l} - \boldsymbol{l}^{ref} \right\|_{\boldsymbol{W}_l}^2 + \left\| \boldsymbol{h} - \boldsymbol{h}^{ref} \right\|_{\boldsymbol{W}_h}^2 \tag{15}$$

IEEE Transactions on Automation Science and Engineering (T-ASE) paper, presented at ICRA 2024, Yokohama, Japan.

where $\boldsymbol{l}^{ref}$ and $\boldsymbol{h}^{ref}$ are the reference centroidal linear and angular momentum trajectory, respectively, $\boldsymbol{W}_l$ and $\boldsymbol{W}_h$ are positive definite diagonal weighted matrix.

2) Contact Force Regularization: The rate of the centroidal state is directly determined by the contact forces. Consequently, the contact force regularization is incorporated into the objective function to encourage the contact force to be distributed as evenly as possible

$$\Gamma_f = \sum_i \sum_j \left\| \boldsymbol{f}_i^j \right\|_{\boldsymbol{W}_f}^2 \tag{16}$$

where $\boldsymbol{W}_f$ is a positive definite diagonal weighted matrix. The weight of the contact force is usually at least three orders of magnitude smaller than the weights of the centroidal state.

The constraints include equality constraints of the centroidal dynamics that are similar to those of (11) and boundary constraints of the non-negative factor of the contact forces:

$$\begin{cases} \alpha_{i,j}^s \geq 0, & \Lambda_i^j(t) = 1 \\ \alpha_{i,j}^s = 0, & \Lambda_i^j(t) = 0 \end{cases} \tag{17}$$

which enforces only the lower bound of $\alpha_{i,j}^s$ when the contact is active and restricts it equal to 0 when it is not active.

C. Nonlinear Centroidal MPC Formulation

Based on the above objective function and constraints (Section III-B), combined with the nonlinear centroidal prediction model (Section III-A), the nonlinear MPC problem is formulated and then transcribed into a NLP by the direct collocation method. The sampling time of the NC-MPC is predefined from the offline trajectory, and the prediction horizon contains N samples. The NC-MPC formulation can be written as

$$\min_{\boldsymbol{x}[k],\boldsymbol{u}[k]} \quad \sum_{k=0}^{N-1} \left(\Gamma_{CoM} + \Gamma_{CM} + \Gamma_f\right) \Delta T(k) \tag{18a}$$

$$\text{s.t.} \quad \boldsymbol{x}[0] = \boldsymbol{x}^{est},\ t[k] = \sum_{e=0}^{k} \Delta T(e) \tag{18b}$$

$$\dot{\boldsymbol{x}}[k] = f_{CenDyn}(t[k], \boldsymbol{x}[k], \boldsymbol{u}[k]) \tag{18c}$$

$$\boldsymbol{x}[k+1] = \boldsymbol{x}[k] + \frac{\dot{\boldsymbol{x}}[k+1] + \dot{\boldsymbol{x}}[k]}{2} \Delta T(k) \tag{18d}$$

$$\begin{cases} \alpha_{i,j}^s[k] \geq 0, & \Lambda_i^j(t[k]) = 1 \\ \alpha_{i,j}^s[k] = 0, & \Lambda_i^j(t[k]) = 0 \end{cases} \tag{18e}$$

where $\boldsymbol{x}[k]$ and $\boldsymbol{u}[k]$ are the centroidal state and a bunch of non-negative factors of the contact forces at the time instant $t[k]$, $\Delta T(k)$ is the k-th sample interval, $\boldsymbol{x}^{est}$ denotes the estimated initial robot's centroidal state of prediction horizon, f_{CenDyn} is the nonlinear centroidal dynamics, the trapezoid method is used to approximate the dynamics constraints (18d).

The performance of nonlinear MPC is significantly determined by the initial guess. The optimized template behavior is a nice initial guess and used to warm up the NC-MPC. Compared to assigning the centroidal momentum trajectory directly to zero in [29], our NC-MPC requires fewer iterations to converge to a near local minimum.

IV. Simulation and Experiment Results

In this section, we present some simulation and experimental results about the optimized behaviors using the synthesis of the EBG and the NC-MPC. We have built some challenging non-flat scenarios both in simulation and the real world. With the humanoid robot BHR7P [37], the optimized dynamic motions are implemented to verify the effectiveness of the proposed methods. These behaviors in this section are visible in the accompanying video.

A. Robot Model and Experimental Setup

The humanoid robot BHR7P is a position-controlled robot with a total weight of 55.9 kg and a height of 1.4 m. It has a total of 14 actuated joints (6 for each leg, 1 for each arm). There exists a nonlinear coupling between the knee joint provided by a particular four-bar actuation mechanism and ankle joints driven by a parallel mechanism. This is taken into account as a nonlinear constraint in TO.

The EBG is performed offline on a laptop with an Intel (R) Core (TM) i7-7700 CPU @ 3.60GHz. The transcribed NLP is solved numerically by the open-source Interior Point Method solver IPOPT [40]. The gradients of the objective function and the Jacobian of the constraints are also provided to the solver analytically, which drastically boosts the iteration speed of the NLP. Moreover, since the trapezoid method is used for transcription, the NLP problem is sparse despite its large scale. The NC-MPC is performed online and solved in a similar manner.

All simulation experiments are performed in the CoppeliaSim software [41]. The control tick is 5 ms in both simulation and hardware.

B. Template Behaviors Generated by EBG

To test the generality of the proposed behavior generator, we construct four challenging scenarios and generate different dynamic behaviors as shown in Figs. 5-8. The four behaviors are described as follows:

- Stairs climbing: The robot must climb stairs dynamically to the desired platform.
- Slope climbing: The robot must climb a slope to the desired platform.
- Running: The robot must run over the discrete tilted terrain.
- Gap jumping: The robot must jump over a gap.

1) The Configuration of TO: The terrain information of the four scenarios are given. The nominal footholds and contact sequence are also provided in advance. The goal of TO is to optimize the physically feasible whole-body motion and contact forces from the initial state to the desired state.

The constraints (10b)-(10k) described in OCP (10) are discretized at each time knot and subsequently taken as the constraints for the transcribed NLP. Note that when optimizing different behaviors, we only change the allowable range of the local footholds (10c) and the feet complementary constraints (10f)-(10g) based on the terrain information, while the other constraints remain unchanged.

IEEE Transactions on Automation Science and Engineering (T-ASE) paper, presented at ICRA 2024, Yokohama, Japan.

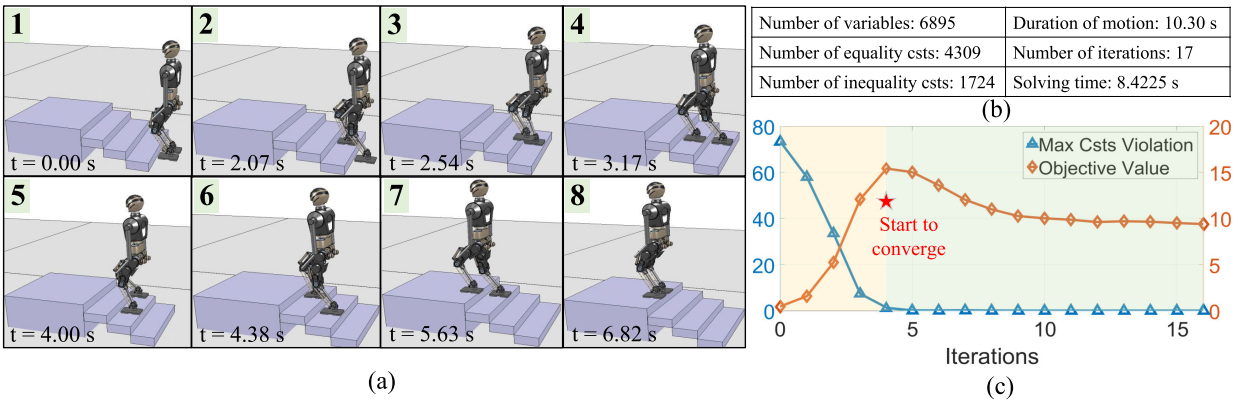

Fig. 5. Behavior 1 - Climbing stairs. (a) Snapshots of simulation. (b) NLP specifications. (c) TO performance.

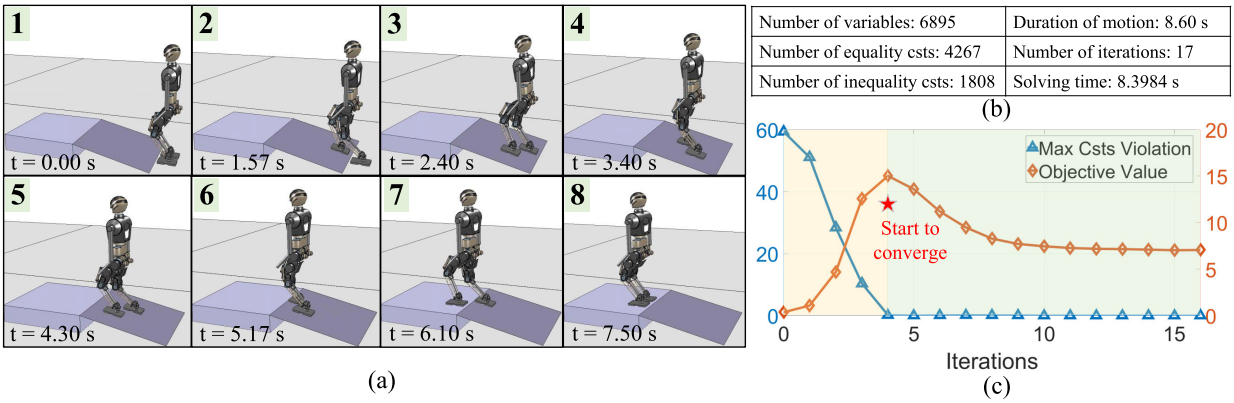

Fig. 6. Behavior 2 - Climbing a slope. (a) Snapshots of simulation. (b) NLP specifications. (c) TO performance.

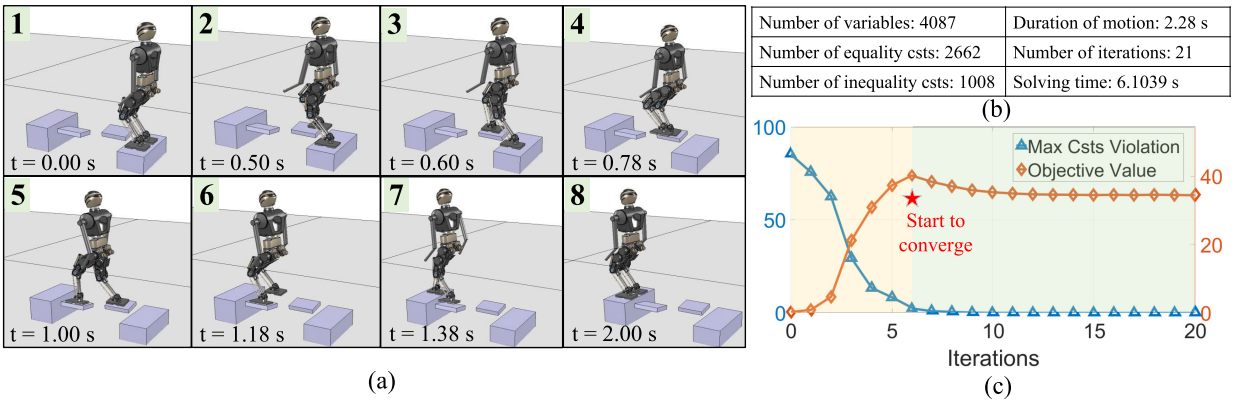

Fig. 7. Behavior 3 - Running pass tilted terrain. (a) Snapshots of simulation. (b) NLP specifications. (c) TO performance.

In nonlinear trajectory optimization, the penalty terms of the objective function and their weights often require many trials to arrive at a relatively appropriate result. Moreover, it is common to trial different objective functions when the optimizing behaviors differ. Sometimes it is frustrating to do this work. As a consequence, in this paper, we exploit a generic objective function (10a) for optimizing different behaviors, including penalty terms and their weight scaling. Table I presents the penalty terms of the proposed objective function, their corresponding representation, and proper weight scaling obtained by trial and error.

The following items explain why these penalty terms are chosen as components of the proposed objective function and how to set their weights:

- With reference to the variation of the centroidal angular momentum and the acceleration of CoM during human walking [39], we expect that these quantities do not change drastically during robot moving, so we take them as penalty terms and give them relatively large weights.
- We incorporate the contact forces into the objective function as well, in order to allow the contact forces to be distributed evenly and to avoid very large contact forces,

IEEE Transactions on Automation Science and Engineering (T-ASE) paper, presented at ICRA 2024, Yokohama, Japan.

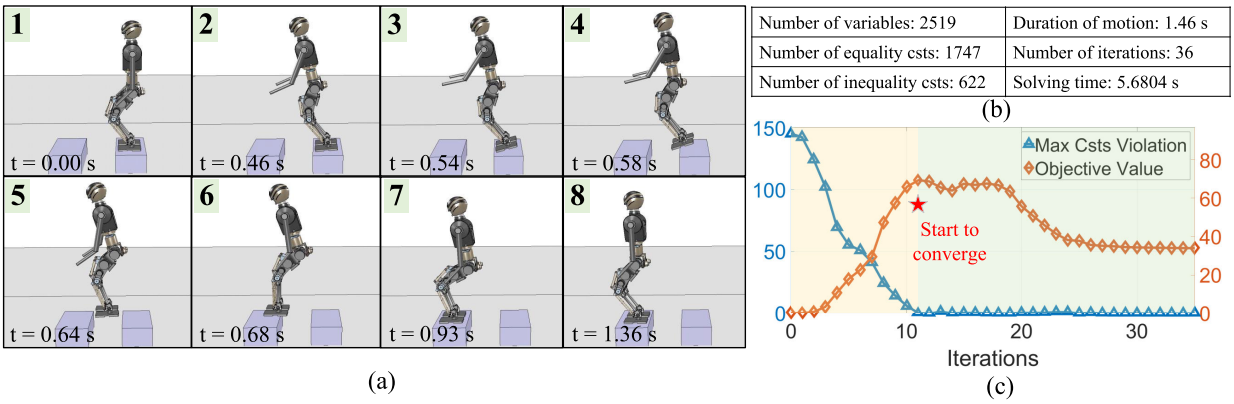

Fig. 8. Behavior 4 - Jumping a gap. (a) Snapshots of simulation. (b) NLP specifications. (c) TO performance.

TABLE I

THE PENALTY TERMS OF OBJECTIVE FUNCTION AND THEIR WEIGHT SCALING

Penalty Terms	Representation	Weights
Centroidal angular momentum regularization	$\boldsymbol{h}^T \boldsymbol{Q}_h \boldsymbol{h}$	1e-1
CoM acceleration regularization	$\ddot{\boldsymbol{c}}^T \boldsymbol{Q}_{\ddot{c}} \ddot{\boldsymbol{c}}$	1e+0
Contact force regularization	$\sum_i \boldsymbol{f}_i^T \boldsymbol{Q}_f \boldsymbol{f}_i$	1.2e-5
Generalized position deviation	$\tilde{\boldsymbol{q}}^T \boldsymbol{Q}_q \tilde{\boldsymbol{q}}$	1e+0

which possibly damage the robot. Since the magnitude of the contact forces is at least two orders of magnitude larger compared to the magnitude of the angular momentum and CoM acceleration, we set a relatively small weight for the contact force regularization.

- The penalty for the generalized position deviation is to keep the robot's generalized position as close as possible to the given reference state. We do not expect the robot to have undesired poses, which would be detrimental to a robot with strict physical joint limits, so we set a relatively large weight for it.

It can be observed from the simulation results (Figs. 5-8) that, at present, the variations in centroidal angular momentum of the current optimized behaviors are relatively gentle. If we want to plan behaviors with significant changes in centroidal angular momentum, such as backflips, it is required to adjust the penalty terms and their weights of the current objective function. Additionally, if necessary, we possibly have to incorporate new penalty terms into the objective function to optimize such dynamic behaviors.

2) The Feasibility of Template Behaviors: Figs. 5(a)-8(a) show the snapshots of four optimized behaviors in simulation. Considering the cumulative error, such as modeling error and sensor noise, which possibly leads to the robot's fall, we combine the NC-MPC as described in Section III with the whole-body control proposed in our previous work [38] to execute climbing stairs and the slope. As for the running and jumping behaviors, unlike walking, we send the optimized joint position directly to the robot in the simulator at each control tick. On the one hand, it is non-trivial to control the dynamic movements with full-flight phases. On the other hand, the optimized behaviors can be executed stably in simulation even without online control, which highlights the feasibility of the optimized behaviors.

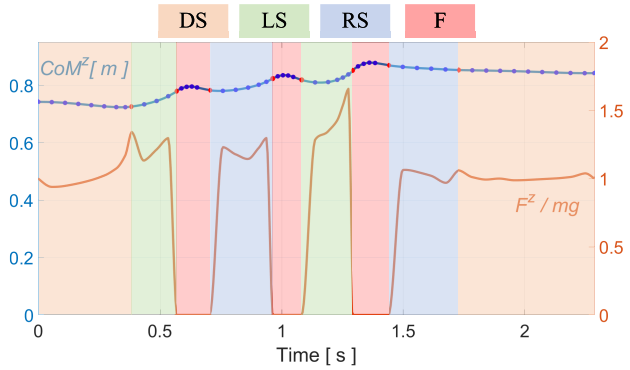

Fig. 9. The optimized vertical CoM position and normalized contact force of running behavior. The different phases are represented by different backgrounds: Double Support (DS, orange), Left Support (LS, green), Right Support (RS, blue), and Flight (F, red).

Fig. 9 illustrates the optimized vertical CoM position and normalized contact force of Behavior 3 as shown in Fig. 7. The robot is expected to run from a platform with a height of 0.2 m through two discrete inclined contact surfaces of incremental height, with inclination angles of -10 degrees and 10 degrees, and finally reach the target platform with a height of 0.3 m. The markers on the vertical CoM curve indicate the optimized CoM height at each time knot. The vertical contact force is interpolated using the method proposed in [42].

Fig. 10 presents the variation of centroidal angular momentum when jumping a gap. The robot is requested to jump a gap to a platform located 0.6 m in front of it, and the desired landing footholds are fixed in the optimization. It shows that only the angular momentum in the sagittal plane changes, while the ones in the lateral and transverse planes stay close to 0, which is attributed to the inclusion of the penalty term for the centroidal angular momentum in the objective function. The arm swinging is automatically generated by TO.

3) The Performance of TO: One of the main concerns of nonlinear optimization is the solution time. It is usually

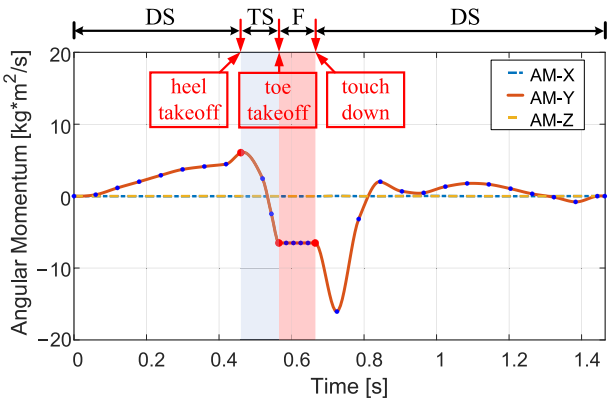

Fig. 10. The variation of the centroidal angular momentum when jumping a gap. The overall jumping behavior includes four successive phases: Double Support (DS), Toe Support (TS), Flight (F), and Double Support (DS). Switching between adjacent phases is accompanied by events (red arrows) in the following order: heel takeoff, toe takeoff, and touch down.

determined by several factors, such as the scale of the problem, the initial guesses, etc. We observe that the proposed objective function and feet complementary constraints can significantly contribute to the convergence of the NLP. Even if the transcribed NLP has a large scale, i.e., thousands of decision variables and constraints (Figs. 5(b)-8(b)), and the provided initial guess is intuitive and very simple, e.g., linear interpolation from the initial state to the desired state, the NLP can still converge to a near-optimal solution after several iterations within seconds.

Taking the walking behavior optimization as an example, the detailed values for the initial guess of decision variables are given by

- Time interval: $\Delta t[i] = T/N$, where T is the guessed total duration of the behavior, and N is the number of discrete knots.
- CoM: The initial guess is the linear interpolation from the initial CoM to the desired CoM.
- Centroidal linear and angular momentum: The initial guess is set to zeros.
- Footholds: The initial guess is set to zeros. Note that it represents that the difference in distance between the nominal contact and the optimized contact, expressed in the local frame of the i-th foot, is equal to zeros. It means that the initial guess of the footholds is the nominal footholds.
- Non-negative factors of the contact forces: The initial guess is equal to $1/32$ of the robot's total weight when planning walking behaviors. Note that when planning dynamic running or jumping behaviors, it can be set equal to $1/16$ of the robot's total weight. Their magnitudes are directly proportional to the magnitudes of the contact forces.
- Generalized position and velocity of the robot: The initial guess of the generalized position is the linear interpolation from the initial state to the desired final state, and the initial guess of the generalized velocity is set to zeros.

From the above detailed initial guess of decision variables, it is observed that they are intuitive and simple. Figs. 5(c)-8(c) depict the iterations of the NLP solver *versus* the maximal constraints (*abbr:* csts) violation and the objective value when optimizing the above behaviors.

It is worth noting that when optimizing the walking behaviors, i.e., climbing stairs and a slope, after only 5 iterations, the maximal constraint violation drops rapidly to a very small value close to 0. Interestingly, the objective value simultaneously reaches its maximum at this time, and then it goes through several more iterations with rapid decline and eventually plateaus. Only a few more iterations are required for the dynamic running and jumping behavior compared to the optimization for walking. These results illustrate that our proposed TO is close to the local feasible domain of attraction.

C. Online Adaptive Motion Generation With NC-MPC

1) The Configuration of the NC-MPC: We develop the MPC controller by exploiting nonlinear centroidal dynamics. The NC-MPC takes the proper optimized behavior as the initial guess, i.e., the warm-start, and regenerates the adaptive behavior online, where the local environment of the robot and footholds are allowed to be different from that in the TO.

Assuming that the local terrain information and the desired footholds are provided by the high-level contact planner, the NC-MPC recomputes the centroidal motion including the CoM position and momentum, and contact forces. The step timings are kept consistent with the offline plans. The weight matrix settings for the penalty terms in the objective function of the NC-MPC are provided as follows:

- $\boldsymbol{W}_{CoM} = diag([1.0, 1.0, 1.0])$
- $\boldsymbol{W}_{l} = diag([0.01, 0.01, 0.01])$
- $\boldsymbol{W}_{h} = diag([0.1, 0.5, 0.1])$
- $\boldsymbol{W}_{f} = diag([0.6e-5, 0.6e-5, 0.6e-5])$

2) Experiment 1 - Climbing Stairs: The consistent physical environment as shown in Behavior 1 is constructed and the online desired footholds are also consistent with those of the behavior generator. Combined with the NC-MPC, the robot continuously performs the stair-climbing task. Thanks to the inclusion of whole-body kinematics in TO, the large range of motion of the feet can be optimized within a relatively small RoM of joints. Fig. 11 presents the snapshots of the humanoid robot BHR7P continuously climbing 4 stairs.

Fig. 13 shows the variations of the robot's CoM height (top) and the vertical Ground Reaction Force (GRF) of the right foot (bottom) during climbing stairs. The NC-MPC is warm-started by the optimized trajectory and then the regenerated centroidal trajectory is tracked by the low-level whole body controller [38]. Since the real-built scenario is consistent with the configuration in TO, the centroidal trajectory and contact forces generated by the NC-MPC are close to the quantities optimized by the EBG.

3) Experiment 2 - Climbing a Slope: In Experiment 1, the synthesis of the offline optimized behavior and online NC-MPC is effective when the actual scenario and desired footholds are consistent with those in EBG. To further verify the effectiveness of the proposed approach, we construct several scenarios with different tilted angles slope in the simulation, successively with 6 degrees, 8 degrees, 10 degrees, 12 degrees, and 14 degrees. It is expected that when the robot

IEEE Transactions on Automation Science and Engineering (T-ASE) paper, presented at ICRA 2024, Yokohama, Japan.

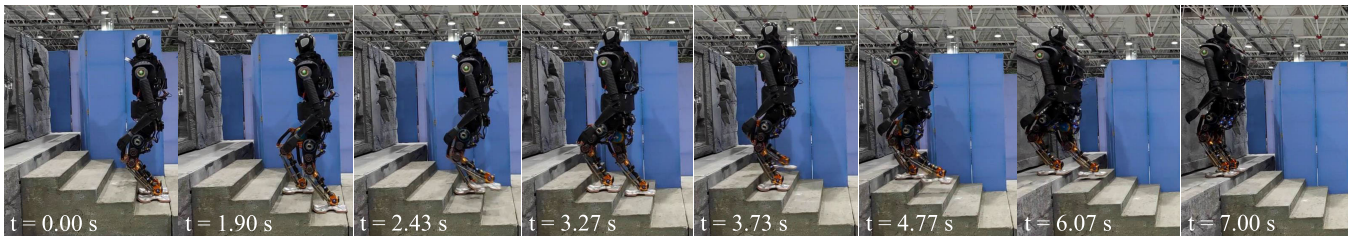

Fig. 11. Experiment 1 - Snapshots of climbing 4 stairs. Each stair has a height of 10 cm, a width of 1 m, and a length of 27 cm.

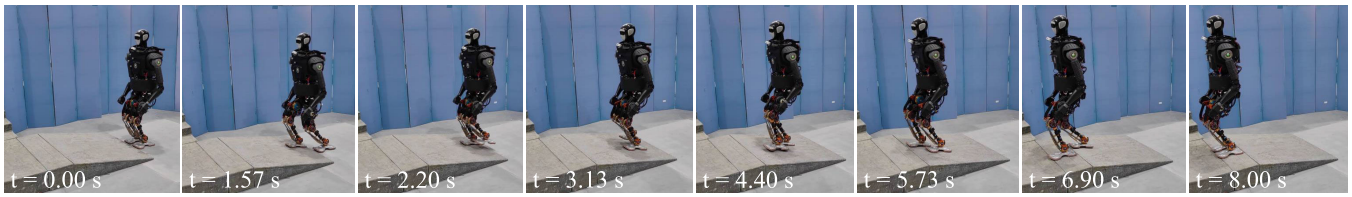

Fig. 12. Experiment 2 - Snapshots of climbing a slope of 12 degrees. The slope has a length of 1 m, and a width of 1 m.

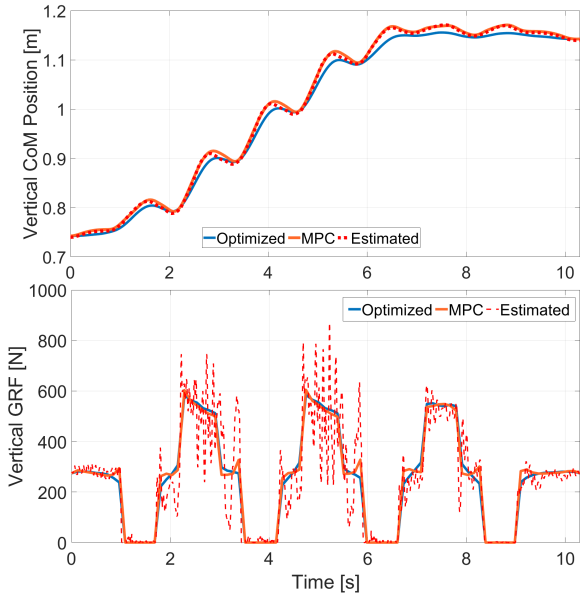

Fig. 13. The offline optimized (blue solid line), MPC (orange solid line), and the estimated (red dotted line) variations of the vertical CoM position (top) and the vertical GRF of the right foot (bottom) during climbing stairs.

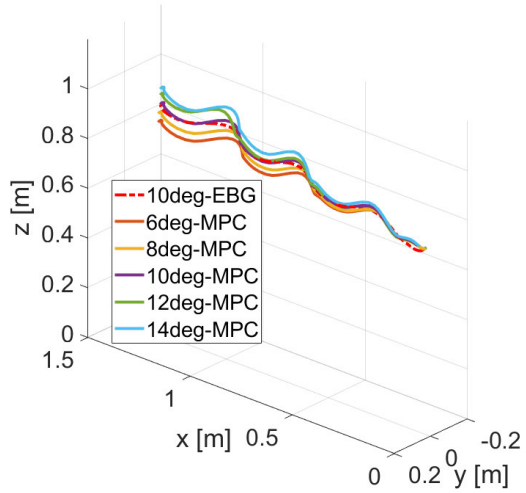

Fig. 14. The CoM trajectories of the robot BHR7P when climbing slopes with different tilted angles in the simulation.

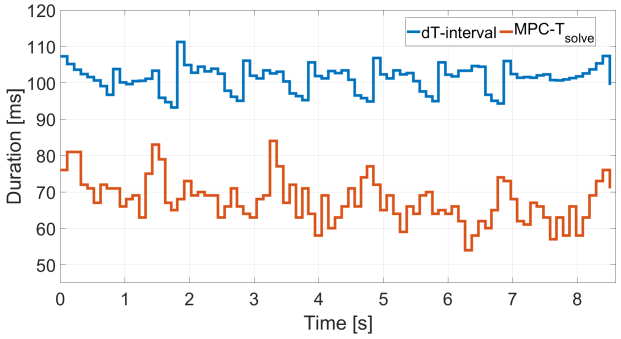

Fig. 15. The intervals (ΔT) of the adjacent time knots and the computation time (T_{solve}) of the NC-MPC during climbing the slope of 12 degrees.

encounters different tilted angles and footholds, the NC-MPC enables the robot to regenerate adaptive motions online via extending a template behavior, e.g., the behavior of climbing a slope with 10 degrees (Behavior 2).

The accompanying video shows how the robot implement the NC-MPC to regenerate adaptive motion and contact forces based on the initial guess and estimated centroidal state, as well as the execution in the simulation. Fig. 12 depicts the snapshots of the humanoid robot BHR7P climbing a slope of 12 degrees. Fig. 14 illustrates the CoM trajectories regenerated by the NC-MPC when BHR7P climbs slopes with different tilted angles in the simulation.

The solving speed of the NC-MPC is one of the main concerns about online execution. In the two experiments shown above, the length of the prediction horizon of the NC-MPC is given as the sum of 12 time-intervals (ΔT) which are obtained by offline TO. The transcribed NLP of the NC-MPC contains 492 decision variables and 108 equality constraints. Warm-started by the nice initial guess, i.e., optimized template behaviors, the NLP can converge to a near local minimum within less than 5 iterations. The NC-MPC takes less than 85ms, also less than the interval (ΔT), to evaluate the outputs of each sampling in Experiment 2, as illustrated in Fig. 15.

V. Discussion

As widely recognized, achieving stable motion for humanoid robots on non-flat terrain is challenging. This

depends not only on the robustness of the control algorithm but also on the hardware and the desired behaviors to be implemented. While the proposed method can generate adaptive behaviors online for the humanoid robot, there are still some limitations derived from the experimental results, which are summarized as follows:

1) The current MPC lacks the capability to adjust the footholds online, which potentially hinders the robot from robustly reacting to intense external perturbations.

2) In the scenarios involving high dynamic behaviors, such as running and jumping, the solving speed of the proposed nonlinear centroidal MPC is not sufficient to generate online adaptive behaviors.

As for the future work, some potential solutions to eliminate the above limitations are considered:

1) A potential solution involves an extension of the proposed MPC. This entails incorporating the footholds as decision variables within the MPC formulation, which allows for the online adjustment of the footholds without changing the predetermined contact sequences.

2) A viable approach centers on the structural refinement of the MPC problem. This involves leveraging the optimized template behavior trajectory to linearize the nonlinear MPC, thereby enhancing its computational efficiency.

VI. Conclusion

In this paper, we present an online motion planner that subtly composes offline optimized behaviors with online reactive motion planning to generate adaptive motions online for humanoid locomotion on non-flat terrain via template behavior extension.

Firstly, we design a generic and efficient behavior generator. When provided with terrain information and nominal footholds, together with the proposed tailored feet complementary constraints, it can efficiently generate physically feasible whole-body template behaviors for humanoid robots, including walking, running, and jumping. Moreover, it can converge to a near-optimal solution in several iterations within a few seconds, even with an intuitive initial guess.

Secondly, we propose an online nonlinear centroidal MPC to enhance the extensibility of template behaviors. Warm-started by the appropriate template trajectories, the NC-MPC is capable of regenerating adaptive centroidal motions and contact forces online according to the actual local terrain information and desired footholds. It properly integrates the motion planner into the closed loop of online control and reveals the potential of the humanoid robot to dynamically traverse non-flat terrain with a sparse template behavior library.

Finally, combined with the proposed method, the humanoid robot BHR7P can dynamically traverse non-flat terrain in simulations and experiments, which demonstrates the validity of the approach.

References

[1] S. Kajita et al., "Biped walking pattern generation by using preview control of zero-moment point," in *Proc. IEEE Int. Conf. Robot. Autom.*, Jul. 2003, pp. 1620–1626.

[2] T. Takenaka, T. Matsumoto, and T. Yoshiike, "Real time motion generation and control for biped robot-1st report: Walking gait pattern generation," in *Proc. IEEE/RSJ Int. Conf. Intell. Robots Syst.*, Oct. 2009, pp. 1084–1091.

[3] J. Englsberger, C. Ott, and A. Albu-Schäffer, "Three-dimensional bipedal walking control based on divergent component of motion," *IEEE Trans. Robot.*, vol. 31, no. 2, pp. 355–368, Apr. 2015.

[4] S. Caron, A. Escande, L. Lanari, and B. Mallein, "Capturability-based pattern generation for walking with variable height," *IEEE Trans. Robot.*, vol. 36, no. 2, pp. 517–536, Apr. 2020.

[5] K. Chappellet, M. Murooka, G. Caron, F. Kanehiro, and A. Kheddar, "Humanoid loco-manipulations using combined fast dense 3D tracking and SLAM with wide-angle depth-images," *IEEE Trans. Autom. Sci. Eng.*, early access, Jun. 14, 2023, doi: 10.1109/TASE.2023.3283497.

[6] S. Kuindersma et al., "Optimization-based locomotion planning, estimation, and control design for the atlas humanoid robot," *Auto. Robots*, vol. 40, no. 3, pp. 429–455, Mar. 2016.

[7] Q. Li et al., "Contact force/torque control based on viscoelastic model for stable bipedal walking on indefinite uneven terrain," *IEEE Trans. Autom. Sci. Eng.*, vol. 16, no. 4, pp. 1627–1639, Oct. 2019.

[8] T. Koolen et al., "Design of a momentum-based control framework and application to the humanoid robot atlas," *Int. J. Humanoid Robot.*, vol. 13, no. 1, Mar. 2016, Art. no. 1650007.

[9] J. Ding, L. Han, L. Ge, Y. Liu, and J. Pang, "Robust locomotion exploiting multiple balance strategies: An observer-based cascaded model predictive control approach," *IEEE/ASME Trans. Mechatronics*, vol. 27, no. 4, pp. 2089–2097, Aug. 2022.

[10] C. Yao, C. Liu, L. Xia, M. Liu, and Q. Chen, "Humanoid adaptive locomotion control through a bioinspired CPG-based controller," *Robotica*, vol. 40, no. 3, pp. 762–779, Mar. 2022.

[11] M. Vukobratović and B. Borovac, "Zero-moment point–thirty five years of its life," *Int. J. Humanoid Robot.*, vol. 1, no. 1, pp. 157–173, 2004.

[12] C. Brasseur, A. Sherikov, C. Collette, D. Dimitrov, and P.-B. Wieber, "A robust linear MPC approach to online generation of 3D biped walking motion," in *Proc. IEEE-RAS 15th Int. Conf. Humanoid Robots (Humanoids)*, Nov. 2015, pp. 595–601.

[13] S. Mason, N. Rotella, S. Schaal, and L. Righetti, "An MPC walking framework with external contact forces," in *Proc. IEEE Int. Conf. Robot. Autom. (ICRA)*, May 2018, pp. 1785–1790.

[14] I. Mordatch, E. Todorov, and Z. Popović, "Discovery of complex behaviors through contact-invariant optimization," *ACM Trans. Graph.*, vol. 31, no. 4, pp. 1–8, Aug. 2012.

[15] G. Schultz and K. Mombaur, "Modeling and optimal control of human-like running," *IEEE/ASME Trans. Mechatronics*, vol. 15, no. 5, pp. 783–792, Oct. 2010.

[16] T. Erez and E. Todorov, "Trajectory optimization for domains with contacts using inverse dynamics," in *Proc. IEEE/RSJ Int. Conf. Intell. Robots Syst.*, Oct. 2012, pp. 4914–4919.

[17] P. B. Wieber, "Holonomy and nonholonomy in the dynamics of articulated motion," in *Fast Motions in Biomechanics and Robotics*. Cham, Switzerland: Springer, 2006, pp. 411–425.

[18] A. Herzog, N. Rotella, S. Mason, F. Grimminger, S. Schaal, and L. Righetti, "Momentum control with hierarchical inverse dynamics on a torque-controlled humanoid," *Auto. Robots*, vol. 40, no. 3, pp. 473–491, Mar. 2016.

[19] D. E. Orin, A. Goswami, and S.-H. Lee, "Centroidal dynamics of a humanoid robot," *Auto. Robots*, vol. 35, nos. 2–3, pp. 161–176, Oct. 2013.

[20] J. T. Betts, "Practical methods for optimal control and estimation using nonlinear programming," in *Society for Industrial and Applied Mathematics*. Philadelphia, PA, USA: SIAM, 2010.

[21] H. Dai, A. Valenzuela, and R. Tedrake, "Whole-body motion planning with centroidal dynamics and full kinematics," in *Proc. IEEE-RAS Int. Conf. Humanoid Robots*, Nov. 2014, pp. 295–302.

[22] J. Carpentier, S. Tonneau, M. Naveau, O. Stasse, and N. Mansard, "A versatile and efficient pattern generator for generalized legged locomotion," in *Proc. IEEE Int. Conf. Robot. Autom.*, May 2016, pp. 3555–3561.

[23] A. W. Winkler, C. D. Bellicoso, M. Hutter, and J. Buchli, "Gait and trajectory optimization for legged systems through phase-based end-effector parameterization," *IEEE Robot. Autom. Lett.*, vol. 3, no. 3, pp. 1560–1567, Jul. 2018.

[24] L. Wang et al., "Design and dynamic locomotion control of quadruped robot with perception-less terrain adaptation," *Cyborg Bionic Syst.*, vol. 2022, Feb. 2022, Art. no. 9816495, doi: 10.34133/2022/9816495.

[25] R. Budhiraja, J. Carpentier, and N. Mansard, "Dynamics consensus between centroidal and whole-body models for locomotion of legged robots," in *Proc. IEEE Int. Conf. Robot. Autom.*, Jul. 2019, pp. 6727–6733.

[26] H. Dai and R. Tedrake, "Planning robust walking motion on uneven terrain via convex optimization," in *Proc. IEEE-RAS 16th Int. Conf. Humanoid Robots (Humanoids)*, Nov. 2016, pp. 579–586.

[27] B. Ponton, M. Khadiv, A. Meduri, and L. Righetti, "Efficient multi-contact pattern generation with sequential convex approximations of the centroidal dynamics," *IEEE Trans. Robot.*, vol. 37, no. 5, pp. 1661–1679, Oct. 2021.

[28] A. Meduri, P. Shah, J. Viereck, M. Khadiv, I. Havoutis, and L. Righetti, "BiConMP: A nonlinear model predictive control framework for whole body motion planning," *IEEE Trans. Robot.*, vol. 39, no. 2, pp. 905–922, Apr. 2023.

[29] G. Romualdi, S. Dafarra, G. L'Erario, I. Sorrentino, S. Traversaro, and D. Pucci, "Online non-linear centroidal MPC for humanoid robot locomotion with step adjustment," in *Proc. Int. Conf. Robot. Autom. (ICRA)*, May 2022, pp. 10412–10419.

[30] Q. Nguyen, X. Da, J. W. Grizzle, and K. Sreenath, "Dynamic walking on stepping stones with gait library and control barrier functions," in *Algorithmic Foundations of Robotics XII*. Cham, Switzerland: Springer, 2020, pp. 384–399.

[31] Y. Guo, M. Zhang, H. Dong, and M. Zhao, "Fast online planning for bipedal locomotion via centroidal model predictive gait synthesis," *IEEE Robot. Autom. Lett.*, vol. 6, no. 4, pp. 6450–6457, Oct. 2021.

[32] S. Tonneau, A. Del Prete, J. Pettré, C. Park, D. Manocha, and N. Mansard, "An efficient acyclic contact planner for multiped robots," *IEEE Trans. Robot.*, vol. 34, no. 3, pp. 586–601, Jun. 2018.

[33] M. Posa, C. Cantu, and R. Tedrake, "A direct method for trajectory optimization of rigid bodies through contact," *Int. J. Robot. Res.*, vol. 33, no. 1, pp. 69–81, Jan. 2014.

[34] H. Hirukawa et al., "A universal stability criterion of the foot contact of legged robots—Adios ZMP," in *Proc. IEEE Int. Conf. Robot. Autom.*, May 2006, pp. 1976–1983.

[35] S. Caron, Q. C. Pham, and Y. Nakamura, "Leveraging cone double description for multi-contact stability of humanoids with applications to statics and dynamics," in *Robotics: Science and Systems*. San Francisco, CA, USA: Robotics Science and System Foundation, 2015, pp. 1–9.

[36] K. Fukuda and A. Prodon, "Double description method revisited," in *Combinatorics and Computer Science*. Cham, Switzerland: Springer, 1996, pp. 91–111.

[37] Q. Li, F. Meng, Z. Yu, X. Chen, and Q. Huang, "Dynamic torso compliance control for standing and walking balance of position-controlled humanoid robots," *IEEE/ASME Trans. Mechatronics*, vol. 26, no. 2, pp. 679–688, Apr. 2021.

[38] C. Dong et al., "A novel hierarchical control strategy for biped robot walking on uneven terrain," in *Proc. IEEE-RAS 19th Int. Conf. Humanoid Robots (Humanoids)*, Oct. 2019, pp. 140–145.

[39] J. Luo, Y. Zhao, L. Ruan, S. Mao, and C. Fu, "Estimation of CoM and CoP trajectories during human walking based on a wearable visual odometry device," *IEEE Trans. Autom. Sci. Eng.*, vol. 19, no. 1, pp. 396–409, Jan. 2022.

[40] A. Wächter and L. T. Biegler, "On the implementation of an interior-point filter line-search algorithm for large-scale nonlinear programming," *Math. Program.*, vol. 106, no. 1, pp. 25–57, Mar. 2006.

[41] C. Robotics. (2022). *Robot Simulator Coppeliasim*. [Online]. Available: https://www.coppeliarobotics.com/

[42] H. Akima, "A method of bivariate interpolation and smooth surface fitting based on local procedures," *Commun. ACM*, vol. 17, no. 1, pp. 18–20, Jan. 1974.

Xiang Meng received the B.S. degree in mechatronics engineering from the Beijing Institute of Technology, Beijing, China, in 2019. He is currently pursuing the Ph.D. degree with the Intelligent Robotics Institute, School of Mechatronical Engineering, Beijing Institute of Technology.

His research interests include motion generation and control for humanoid robots.

Zhangguo Yu received the B.S. degree in electronics engineering and the M.S. degree in control engineering from the Southwest University of Science and Technology, China, in 1997 and 2005, respectively, and the Ph.D. degree in mechatronics engineering from the Beijing Institute of Technology (BIT), China, in 2009.

He is currently a Professor of Mechanical Engineering with BIT and the Director of the Intelligent Robotics Institute, BIT. His research interests include motion planning and control of biped robots.

Xuechao Chen received the B.S. and Ph.D. degrees in mechatronics engineering from the Beijing Institute of Technology (BIT), Beijing, China, in 2007 and 2013, respectively.

He was a Visiting Student with the Robotics Institute, Carnegie Mellon University, Pittsburgh, PA, USA, in 2012. He is currently a Professor with the School of Mechatronical Engineering, BIT. His research interests include biped locomotion and dynamics.

Zelin Huang received the B.S. and M.S. degrees in mechatronics engineering from the Beijing Institute of Technology, Beijing, China, in 2017 and 2020, respectively. She is currently pursuing the Ph.D. degree with the Intelligent Robotics Institute, School of Mechatronical Engineering, Beijing Institute of Technology.

Her research interests include the control of biped robots.

Fei Meng received the B.S. and Ph.D. degrees in mechatronics engineering from the Beijing Institute of Technology (BIT), Beijing, China, in 2008 and 2016, respectively.

He is currently an Associate Professor with the School of Mechatronical Engineering, BIT. His research interests include motion control and actuator design for bionic robots.

Qiang Huang (Fellow, IEEE) received the B.S. and M.S. degrees in electrical engineering from the Harbin Institute of Technology, Harbin, China, in 1986 and 1989, respectively, and the Ph.D. degree in mechanical engineering from Waseda University, Tokyo, Japan, in 1996.

He was a Research Fellow with the National Institute of Advanced Industrial Science and Technology, Japan, from 1996 to 1999. He was a Research Fellow with The University of Tokyo, Japan, from 1999 to 2000. Since 2000, he has been a Professor with the Beijing Institute of Technology (BIT), China. He is currently the Executive Director of the Beijing Advanced Innovation Center for Intelligent Robots and Systems, BIT. His research interests include biped locomotion and biorobotic systems.